THE JOURNAL OF PHYSICAL CHEMISTRY Letters

Letter

The Role of LiCoO Surface Terminations in Oxygen Reduction and Evolution Kinetics

Binghong Han, Danna Qian, Marcel Risch, Hailong Chen, Miaofang Chi, Ying Shirley Meng, and Yang Shao-Horn

J. Phys. Chem. Lett., **Just Accepted Manuscript** • DOI: 10.1021/acs.jpclett.5b00332 • Publication Date (Web): 22 Mar 2015

The Role of $LiCoO_2$ Surface Terminations in Oxygen Reduction and Evolution Kinetics

Binghong Han,[1,3⁄⁄] Danna Qian,[4⁄⁄] Marcel Risch,[2,3] Hailong Chen,[5] Miaofang Chi,[6] Ying S. Meng,[4] Yang Shao-Horn[1,2,3*]*

AUTHOR ADDRESS:

[1]Department of Materials Science and Engineering, [2] Research Laboratory of Electronics, and [3]Electrochemical Energy Lab, Massachusetts Institute of Technology, Cambridge, Massachusetts 02139, United States

[4]Department of NanoEngineering, University of California San Diego, La Jolla, California 92093, United States

[5]The Woodruff School of Mechanical Engineering, Georgia Institute of Technology, Atlanta, GA 30332, United States

[6]Center for Nanophase Materials Sciences, Oak Ridge National Laboratory, Oak Ridge, Tennessee 37831, United States

AUTHOR INFORMATION

Corresponding Author

* Ying S. Meng, shmeng@ucsd.edu

* Yang Shao-Horn, shaohorn@mit.edu

ABSTRACT

Oxygen reduction reaction (ORR) and oxygen evolution reaction (OER) activities of $LiCoO_2$ nanorods with sizes in the range from 9 to 40 nm were studied in alkaline solution. The sides of these nanorods were terminated with low-index surfaces such as (003) while the tips were terminated largely with high-index surfaces such as (104) as revealed by high-resolution transmission electron microscopy. Electron energy loss spectroscopy demonstrated that low-spin Co^{3+} prevailed on the sides, while the tips exhibited predominantly high- or intermediate-spin Co^{3+}. We correlated the electronic and atomic structure to higher specific ORR and OER activities at the tips as compared to the sides, which was accompanied by more facile redox of $Co^{2+/3+}$ and higher charge transferred per unit area. These findings highlight the critical role of surface terminations and electronic structures of transition metal oxides on the ORR and OER activity.

TOC GRAPHIC

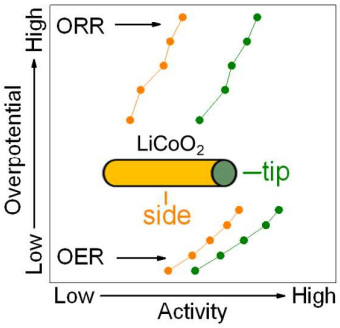

KEYWORDS: Oxygen Evolution Reaction, Oxygen Reduction Reaction, Nanorods, EELS, Lithium Intercalation

Design of highly active catalysts to catalyze the redox of molecular oxygen is critical to realize air-based energy storage in the pursuit of sustainable energy. The kinetics of oxygen reduction reaction (ORR) and oxygen evolution reaction (OER) limit the efficiency of many electrochemical technologies, including proton exchange membrane fuel cells,[1] water splitting[2-5] and rechargeable metal-air batteries.[6-9] Earth-abundant and precious-metal-free transition-metal oxides can catalyze ORR and OER with comparable activities to precious metal-based catalysts in alkaline solution.[8-17] Recent studies have shown that electronic structure features of oxides such as e_g occupancy[13, 18-19] of transition metal ions could govern the ORR/OER activities of transition metal oxides, where having an e_g occupancy close to unity showed maximum specific ORR and OER activity.[13, 18] More recently, it has been found that moving the O p band center closer to the Fermi level leads to much enhanced specific OER activity.[12] In addition, a better flexibility of transition metal atoms to adopt various oxidation and spin configurations is also correlated to higher OER activity.[20] However, these previous studies[12, 16-19] employ oxide powder samples that have undefined surface facets. Therefore, the reported ORR and OER activities represent the averaged activities from all surface facets exposed to the alkaline solution.

Here we examine the role of oxide surface terminations on the ORR and OER activities in alkaline solution using $LiCoO_2$ nanorods, which have been reported recently to have low-spin Co^{3+} on the nanorod sides predominantly terminated by the (003) facet and intermediate- or high-spin Co^{3+} on tips that are usually dominated by high-index surfaces such as (104).[21] The ORR and OER activities and

pseudo-capacitance of these rod-shaped $LiCoO_2$ were studied in 0.1 M KOH. Higher specific ORR and OER activities accompanied by higher charge transferred per surface area during Co 2+/3+ and 3+/4+ redox processes were found at the tips, compared with the side surfaces.

The $LiCoO_2$ nanorods were characterized firstly by transmission electron microscopy (TEM). These nanorods have similar morphologies (Figures 1a and 1b) but different sizes and were denoted by their average diameter of 9, 14, 31 and 40 nm (Figure 1c). The calculation of tip and side surface areas can be found in the supporting information (SI), and the results are shown in Table S1, with tip surface areas ~ 3-9 m^2/g and side surface areas ~ 25-150 m^2/g.

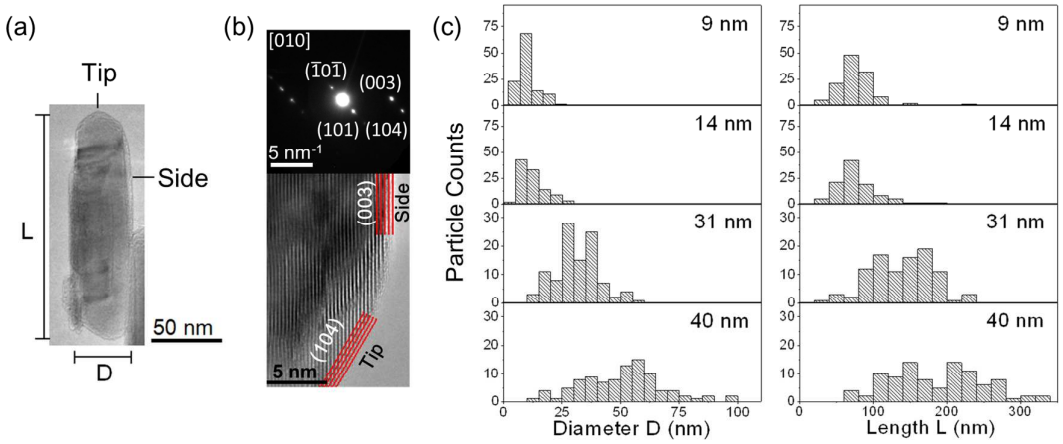

Figure 1. (a) Representative TEM image of a nanorod from the $LiCoO_2$ sample with an average rod diameter of 40 nm. (b) High-resolution TEM image of a representative nanorod $LiCoO_2$ with its associated selected-area electron diffraction pattern. (c) Histograms of the length and diameter distributions of different $LiCoO_2$ samples.

Electron energy loss spectroscopy (EELS) analysis of $LiCoO_2$ nanorods suggested that the tips could have lower hybridization of Co-O bounds than the sides. Representative EELS spectra of the pristine 9-nm sample are shown in Figure 2a and 2b, where the position of EELS acquisition is shown in Figure S2. The Co L_3/L_2 ratios of ~2.7 were comparable to those of our previous XPS results,[21] indicative of Co oxidation state of 3+, and no noticeable changes in the Co L_3/L_2 ratio was observed between side and tip. For O K spectra, the area of the pre-peak was linearly proportional to the product of the total number of the empty O 2p − Co 3d states (4 for Co^{3+} considering equal weighting of e_g and t_{2g} electrons) and their extent of hybridization.[19] The quantitative analysis of the difference of O pre-peak areas between sides and tips can be found in Table S3, where the side of pristine $LiCoO_2$ showed a ~20% larger pre-peak area in the O K-edge than the tip at around 532 eV, consistent with our previous study on $LiCoO_2$ nanorods.[21] The smaller pre-peak on tips suggested an intermediate- or high-spin Co^{3+} with weaker hybridization of O 2p and Co 3d, originated from the under-coordinated Co atoms on tip surfaces (Figure S7b and S7c),[21] while the fully-coordinated Co atoms on nanorod sides (Figure S7a and S7e) have a low-spin state with a greater degree of O 2p and Co 3d hybridization. Such difference in electronic structures between tips and sides could play an important role in surface catalytic reactions, as it is expected to influence the absorption of oxygen.

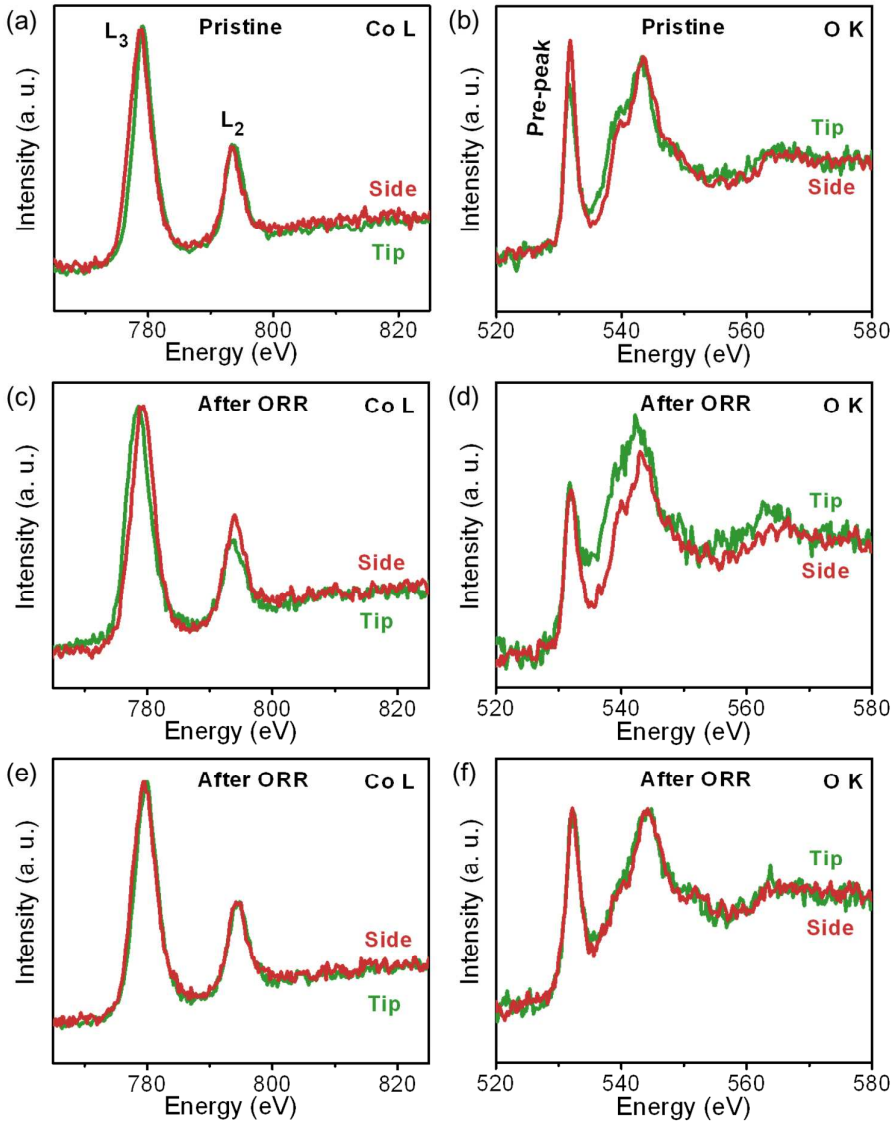

Figure 2. (a)(b) Representative EELS spectra of pristine 9-nm $LiCoO_2$: (a) Co L edge, (b) O K edge. (c)-(f) Two types of representative EELS spectra of 9-nm sample held at 0.7 V vs. RHE for ORR. Middle row is one set of (c) Co L edge and (d) O K edge (case 1); bottom row (e) and (f) is the other set of spectra (case 2). The analysis of O K pre-peak (at 532 eV) intensities can be found in Table S3.

The geometric ORR and OER activity (which is proportional to mass activity in this study due to identical oxide loading) in Figures 3a and 3b suggested that the smaller the particle size, the higher the total activity, due to the higher total surface area of the smaller nanorods. After normalizing by the total surface area, which is usually done by previous works to compare the specific activity,[9, 13, 15, 18] we found that the larger size samples with diameters of 31 and 40 nm have higher ORR activity and slightly higher OER activity than the smaller ones of 9 and 14 nm, as shown in Figures 3c and 3d. However, one cannot assume that the tip and side surfaces of $LiCoO_2$ nanorods have similar OER and ORR activities, and the normalization by total surface area is not accurate. Thanks to the well-defined shape and facet of the $LiCoO_2$ nanorods in this paper, we are able to separate the specific activity of the tip (j_{tip}) from that of the side (j_{side}) using the algebraic method described in the experimental methods. The results in Figure 3e showed that the tip surfaces are ~10 times more active for ORR than the side surfaces. In OER, the tip surfaces are still more active than the side surface (Figure 3f), although the difference (~4 times) is smaller than that in ORR. The tip of $LiCoO_2$ showed comparable specific OER and ORR activities to other active Co-containing micron-sized oxides such as $LaCoO_3$ (see Figure S1). This will be further discussed in the later EELS session.

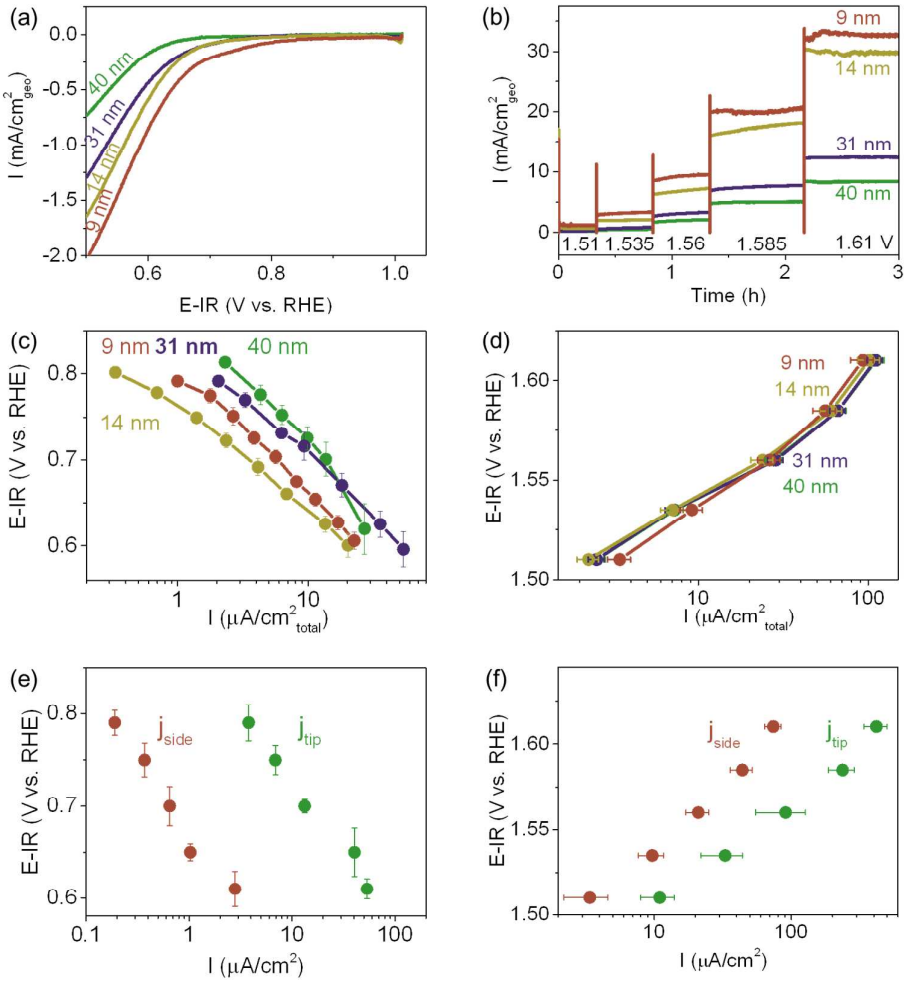

Figure 3. (a) Cyclic voltammetry of ORR current of different $LiCoO_2$ samples in O_2-saturated 0.1 M KOH at 10 mV/s, with a rotation speed of 1600 rpm, after IR and background correction. (b) Potentiostatic measurements of OER current of different $LiCoO_2$ samples in O_2-saturated 0.1 M KOH at different voltages, with rotation speed of 1600 rpm. (c) and (d) Tafel plots of ORR and OER activities of $LiCoO_2$ normalized by total surface area estimated from TEM particle size distribution,[22] respectively. The error bars represent the standard deviation of three different measurements for each sample. (e) and (f) Tafel plots of the specific ORR and OER activities of tip and side surfaces of $LiCoO_2$. The error bars were obtained from linear regression of j_{side} and j_{tip}

(see SI for calculation).

In addition to OER and ORR, the tip of $LiCoO_2$ nanorods was found to be more redox active than the side surfaces in the redox of surface Co atoms. Redox peaks of $LiCoO_2$ in 0.1 M KOH were clearly discernible in the CV at ~1.1 V and ~1.4 V (vs. RHE), respectively (Figure 4). We found that the smaller LiCoO2 samples have Co oxidation and reduction peaks farther departing from the equilibrium potentials, which might be caused by their larger ratios of side surface that is less reactive and/or less surface conductive due to the fully-coordinated surface Co atoms on the sides (Figure S7a). We have shown previously[9] that the redox peaks of $LiCoO_2$ in 0.1 M KOH occur at comparable potentials to other Co compounds such as $LiCoPO_4$, where the Co redox can be coupled mainly to protonation/deprotonation in aqueous solutions[9, 23]. In addition, recent XAS investigations[23-25] of cobalt oxides with oxidation states between 2+ and 4+, show that the redox at the lower potential can be assigned to Co 2+/3+ and the one at higher potentials to 3+/4+. The possible local redox reactions on the surface may be described as follows:[26] $CoOOH + H_2O + e^- \leftrightarrow Co(OH)_2 + OH^-$ for Co 2+/3+, and $CoO_2 + H_2O + e^- \leftrightarrow CoOOH + OH^-$ for Co 3+/4+, where further studies are needed to provide mechanistic details. The amplitude of the Co 2+/3+ redox peaks was larger than the amplitude of the Co 3+/4+ redox peaks for nano-sized $LiCoO_2$ and $LiCoPO_4$. The intensity of the Co 2+/3+ redox peak decreased with increasing particle size, while the trend is opposite for Co 3+/4+, resulting in a larger amplitude of the

latter peak in larger (sub-micron) $LiCoO_2$ particles (Figure 4a). The integration of charge associated with these Co redox processes after double-layer capacitance subtraction (Figure 4b) showed that the charge associated with Co 2+/3+ redox (~1.7 C/m^2) was one order of magnitude larger than that of Co 3+/4+ (~0.17 C/m^2), see Table S2. We can also find that the smaller samples have more charge transferred per unit weight during both redox processes due to their higher surface areas from Table S2. It has been proposed previously that $LiCoO_2$ reduces at the surface in a non-aqueous electrolyte due to Co occupying Li sites while the bulk is unaffected.[27] The resulting spinel-like structure is also supported by in-situ XAS in 0.1 M KOH[24] and has been previously proposed as the active surface for OER[28] and ORR.[17] This surface reduction might explain why the Co 2+/3+ redox is more pronounced in smaller particles with large surface areas. In support of the special roles of open sites on the surface between CoO_2 slabs (Figure S7), the tip surfaces contributed more to the electron transfers during Co redox processes than the side surfaces. An algebraic method was applied to further quantify the contributions from tip and side of the rod. The results are shown in Figure 4c, where the charge transferred per surface area on the tip (q_{tip}) is several times larger than that on the side (q_{side}) for both Co 2+/3+ and 3+/4+ redox processes. The observation suggests that the tip of $LiCoO_2$ can be easier reduced and oxidized as compared to the side surfaces. The considerably higher redox currents and charge associated with Co 2+/3+ found on the tip can be responsible for remarkably higher ORR activity on the tip surfaces. On the other hand, the redox currents and charge of Co 3+/4+ found on the tip might be slightly larger than those

found on the side but considering experimental uncertainty in the analysis, the difference might not be significant. The difference in redox charge associated with Co 3+/4+ found on the tip and side is comparable to the OER activity difference. The surface Co redox can also be confirmed from EELS: after ORR the Co L_3/L_2 ratio increased from original ~2.7 to ~3.8 for tips and to ~3.1 for sides (Figure 2c and Table S5), indicating the partially reduction of surface Co atoms;[29] while after OER, the L_3/L_2 ratio decreased to ~2.5 for tips and is still ~2.7 for sides (Figure S5a and Table S5), indicating the partially oxidation of Co on tips. The change of L_3/L_2 ratios on tips are larger than on sides, and the change after ORR is larger than after OER, which is also in consistent with the result in Figure 4c that shows tips have larger charge transferred per surface area than sides and Co2+/3+ redox process has larger charge transferred than 3+/4+ redox.

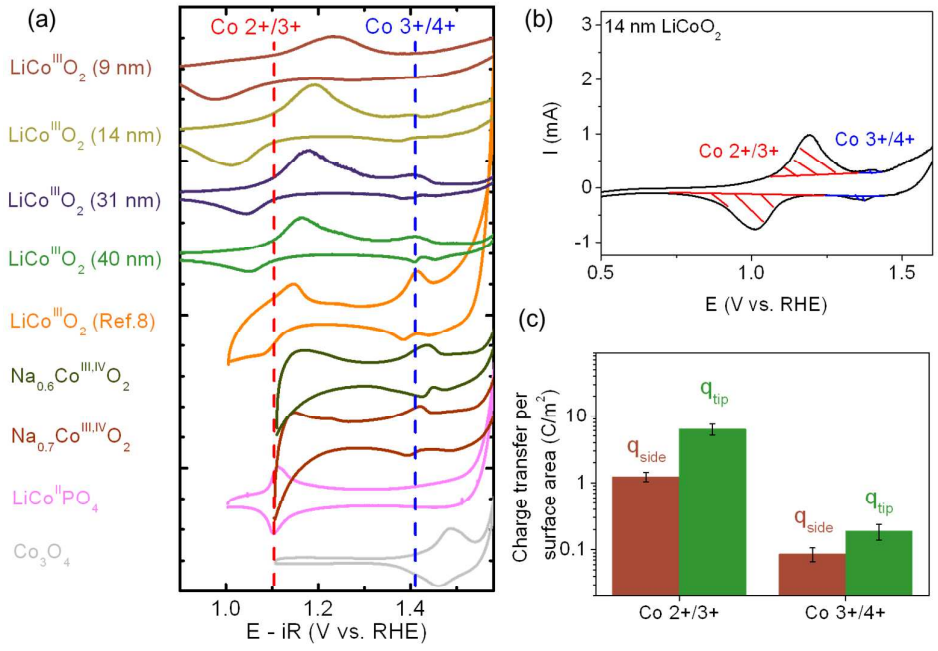

Figure 4. (a) CV curves of different Co compounds in the Co redox region. Each curve is normalized to have similar redox peak height. In $LiCoO_2$ samples, both Co 2+/3+ and 3+/4+ redox peaks can be found around 1.1 and 1.4 V vs. RHE, respectively. (b) Calculation scheme of charge transferred during Co 2+/3+ and 3+/4+ redox reactions by integrating the redox peaks. (c) Charge transferred per surface area of tip and side surfaces of $LiCoO_2$ during 2+/3+ and 3+/4+ redox processes. The error bars were obtained from linear regression of q_{side} and q_{tip} (see SI for calculation).

After ORR or OER measurements (holding at 0.7 or 1.55 V vs. RHE for 1 h), 50% of $LiCoO_2$ nanorods examined were found to have maintained a smaller O K pre-peak on the tip (peak area <3.5, similar to the pristine tip) than that on the side (peak area >4, similar to the pristine side), as shown in Figures 2d, S5b and case 1 in Table S3. This indicates the open structure (Figure S7b) can be at least partially kept during OER and ORR on the tip. This can explain the higher ORR/OER activities of the tip as compared to the side, since the open structure and the under-coordinated Co ions on tips can adsorb oxygen species from the electrolyte more easily (Figure S7d) and therefore could promote ORR kinetics assisted by more facile Co redox via $CoOOH + H_2O + e^- \leftrightarrow Co(OH)_2 + OH^-$ at the side, with the oxygen being more easily to dissociate/intercalate.[13, 18, 20] We also found 50% of the $LiCoO_2$ nanorods showed comparable O K pre-peak areas between tip and side after OER or ORR, all close to the pre-peak of pristine side surface (peak area ~4.5), as shown in Figures 2f, S5d and case 2 in Table S3. This can also be observed in a control experiment with the pristine

sample immersed in O_2-saturated 0.1 M KOH electrolyte for 1 h (Figure S6 and Table S3). This changing of tip pre-peak area is probably due to the under-coordinated surface Co on the tip getting bonded by water or OH/OOH groups (Figure S6e) and then the surface reconstructed, making the coordination and chemical environment of Co atoms on the tip become similar to that on the side. A comparable oxidation of $Co(OH)_2$ in 1 M KOH has been reported previously.[25] During control experiment, the $LiCoO_2$ nanorods statically contacted and adsorbed water or OH/OOH groups for a long time, which led to the gradually reconstruction of all the under-coordinate Co on tips; while during ORR or OER, the OH/OOH group adsorbed on under-coordinate Co ions is continuously consumed and re-adsorbed, and therefore the active Co sites on the tip surface are cyclically regenerated without long-time OH/OOH group adsorption, which might be the reason that only some of the nanorods lost their under-coordinated tips after ORR or OER.

In summary, we report that the tip surface of rod-shaped $LiCoO_2$ nanoparticles, with high index surfaces such as (104), has higher ORR and OER activity as compared to the side with low index surfaces. In addition, the tip surface has larger specific charge transferred than the side for both Co 2+/3+ and 3+/4+ redox processes. The more facile access to oxygen species and easier redox of under-coordinated Co atoms on high-index tip surfaces are used to explain the difference in catalytic performance between tips and sides. These findings showed that the surface catalytic reactions, such as OER and ORR, are closely related to surface terminations that determine the surface atomic and electronic structures of transition metals oxides. Therefore, the

controlling and modification of surface terminations could be an effective way to design future catalysts.

EXPERIMENTAL METHODS

Material preparation and more experimental details can be found in SI.

Electrochemical Measurements. The rotating disk electrode (RDE) configuration was employed for electrochemical measurements. All potentials were calibrated to the reversible hydrogen electrode (RHE) using H_2/H^+ redox. $LiCoO_2$ samples were mixed with the oxides: AB carbon: Nafion® ratio of 5:1:1, and the oxides loading on the disk is 0.25 mg/cm^2_{disk}. All electrochemical measurements were done in 0.1 M KOH, with IR (resistance determined using electrochemical impedance spectroscopy) and double-layer capacitance corrections (see Figure S8) when available. All measurements were repeated 3 times to establish good reproducibility.

Transmission Electron Microscopy. TEM images were taken on JEOL 2010F with a point resolution of 0.19 nm, used to determine particle size distributions and general morphology of the catalyst nanoparticles. High resolution TEM images were formed without an objective aperture and were analyzed using Gatan Digital Micrograph v2.01 (Gatan Inc.). $LiCoO_2$ particles were assumed to have a rod shape with different sizes and are noted using their average diameters of 9nm, 14nm, 31nm and 40 nm,

determined by TEM images. The tip and side surface areas were computed using the particle size distributions collected from TEM images[22] with the method explained in the SI.

Algebraic method to separate tip and side contributions. Assuming tip and side surfaces have different specific activities for OER or ORR, we have:

$$I = S_{tip}j_{tip} + S_{rod}j_{rod} \quad \text{Eq. 1}$$

where I is the measured mass-normalized ORR or OER activity currents at certain voltage, j_{tip} and j_{side} are the specific surface activities on tip and side surfaces, respectively. Here we assume the j_{tip} and j_{side} of samples with different size are the same at each potential, then the two unknowns j_{tip} and j_{side} can be calculated by linear fitting the I, S_{tip} and S_{side} of different-size samples at corresponding potentials. The same method can also be used to compute the contributions of tip and side on charge transferred during Co 2+/3+ and 3+/4+ redox processes. The calculation details and standard error estimation can be found in the SI.

EELS. All EELS spectra were acquired at 60 kV and with a beam size of ~0.7Å, on a Cs-corrected FEI Titan 80/300-kV TEM/STEM microscope equipped with a Gatan Image Filter Quantum-865, except for those of controlling measurements acquired at 300 kV. The energy resolution is around 1eV. For each sample, at least six particles'

spectra were collected. The quantitative analysis of O K-edge can be found in Table S3.

ACKNOWLEDGEMENTS

This work is supported by U.S. Department of Energy, Office of Energy Efficiency and Renewable Energy under grant DE-EE0000458. The research made use of the Shared Experimental Facilities supported by the MRSEC Program of the National Science Foundation under award number DMR 08-019762. The STEM/EELS experiments were carried out through a user project supported by ORNL's Center for Nanophase Materials Sciences (CNMS), which is sponsored by the Scientific User Facilities Division, Office of Basic Energy Sciences, U. S. Department of Energy. The authors thank Dr. Alexis Grimaud for synthesizing and characterizing $NaCoO_2$ in Figure 4A.

ASSOCIATED CONTENT

Supporting Information: EELS measurement scheme, more EELS comparison of 9-nm samples after ORR and OER measurements. Comparison of $LiCoO_2$ activity to other catalysts. XRD results. Tables for the redox charge transfers and specific surface

areas. Detailed experimental information. This material is available free of charge via the Internet at http://pubs.acs.org.

AUTHOR INFORMATION.

Corresponding Author

*E-mail: shaohorn@mit.edu.

*E-mail: shmeng@ucsd.edu

Author Contributions

‖ These authors contributed equally to this work.

REFERENCES

(1) Service, R. F. Hydrogen Cars: Fad or the Future? *Science* **2009,** *324*, 1257-1259.

(2) Gray, H. B. Powering the Planet with Solar Fuel. *Nat. Chem.* **2009,** *1*, 112-112.

(3) Lewis, N. S.; Nocera, D. G. Powering the Planet: Chemical Challenges in Solar Energy Utilization. *Proc. Natl. Acad. Sci.* **2006,** *103*, 15729-15735.

(4) Kanan, M. W.; Nocera, D. G. In Situ Formation of an Oxygen-Evolving Catalyst in Neutral Water Containing Phosphate and Co^{2+}. *Science* **2008,** *321*, 1072-1075.

(5) McCrory, C. C. L.; Jung, S.; Peters, J. C.; Jaramillo, T. F. Benchmarking Heterogeneous Electrocatalysts for the Oxygen Evolution Reaction. *J. Am. Chem. Soc.* **2013,** *135*, 16977-16987.

(6) Lu, Y.-C.; Xu, Z.; Gasteiger, H. A.; Chen, S.; Hamad-Schifferli, K.; Shao-Horn, Y. Platinum−Gold Nanoparticles: A Highly Active Bifunctional Electrocatalyst for Rechargeable Lithium−Air Batteries. *J. Am. Chem. Soc.* **2010,** *132*, 12170-12171.

(7) Armand, M.; Tarascon, J. M. Building Better Batteries. *Nature* **2008,** *451*, 652-657.

(8) Maiyalagan, T.; Jarvis, K. A.; Therese, S.; Ferreira, P. J.; Manthiram, A. Spinel-Type Lithium Cobalt Oxide as a Bifunctional Electrocatalyst for the Oxygen Evolution and Oxygen Reduction Reactions. *Nat. Commun.* **2014,** *5*, 3949 1-8.

(9) Lee, S. W.; Carlton, C.; Risch, M.; Surendranath, Y.; Chen, S.; Furutsuki, S.; Yamada, A.; Nocera, D. G.; Shao-Horn, Y. The Nature of Lithium Battery Materials under Oxygen Evolution Reaction Conditions. *J. Am. Chem. Soc.* **2012,** *134*, 16959-16962.

(10) Risch, M.; Stoerzinger, K. A.; Maruyama, S.; Hong, W. T.; Takeuchi, I.; Shao-Horn, Y. $La_{0.8}Sr_{0.2}MnO_{3-\delta}$Decorated with $Ba_{0.5}Sr_{0.5}Co_{0.8}Fe_{0.2}o_{3-\delta}$: A Bifunctional Surface for Oxygen Electrocatalysis with Enhanced Stability and Activity. *J. Am. Chem. Soc.* **2014,** *136*, 5229-5232.

(11) Stoerzinger, K. A.; Risch, M.; Suntivich, J.; Lu, W. M.; Zhou, J.; Biegalski, M. D.; Christen, H. M.; Ariando; Venkatesan, T.; Shao-Horn, Y. Oxygen Electrocatalysis on (001)-Oriented Manganese Perovskite Films: Mn Valency and Charge Transfer at the Nanoscale. *Energy Environ. Sci.* **2013,** *6*, 1582-1588.

(12) Grimaud, A.; May, K. J.; Carlton, C. E.; Lee, Y.-L.; Risch, M.; Hong, W. T.; Zhou, J.; Shao-Horn, Y. Double Perovskites as a Family of Highly Active Catalysts for Oxygen Evolution in Alkaline Solution. *Nat. Commun.* **2013,** *4*, 2439 1-7.

(13) Suntivich, J.; May, K. J.; Gasteiger, H. A.; Goodenough, J. B.; Shao-Horn, Y. A Perovskite Oxide Optimized for Oxygen Evolution Catalysis from Molecular Orbital Principles. *Science* **2011,** *334*, 1383-1385.

(14) Meadowcroft, D. B. Low-Cost Oxygen Electrode Material. *Nature* **1970,** *226*, 847-848.

(15) Suntivich, J.; Gasteiger, H. A.; Yabuuchi, N.; Shao-Horn, Y. Electrocatalytic Measurement Methodology of Oxide Catalysts Using a Thin-Film Rotating Disk Electrode. *J. Electrochem. Soc.* **2010,** *157*, B1263-B1268.

(16) Lu, Z.; Wang, H.; Kong, D.; Yan, K.; Hsu, P.-C.; Zheng, G.; Yao, H.; Liang, Z.; Sun, X.; Cui, Y. Electrochemical Tuning of Layered Lithium Transition Metal Oxides for Improvement of Oxygen Evolution Reaction. *Nat. Commun.* **2014,** *5*, 4345 1-7.

(17) Maiyalagan, T.; Jarvis, K. A.; Therese, S.; Ferreira, P. J.; Manthiram, A. Spinel-Type Lithium Cobalt Oxide as a Bifunctional Electrocatalyst for the Oxygen Evolution and Oxygen Reduction Reactions. *Nat. Commun.* **2014,** *5*.

(18) Suntivich, J.; Gasteiger, H. A.; Yabuuchi, N.; Nakanishi, H.; Goodenough, J. B.; Shao-Horn, Y. Design Principles for Oxygen-Reduction Activity on Perovskite Oxide Catalysts for Fuel Cells and Metal–Air Batteries. *Nat. Chem.* **2011,** *3*, 546-550.

(19) Suntivich, J.; Hong, W. T.; Lee, Y.-L.; Rondinelli, J. M.; Yang, W.; Goodenough, J. B.; Dabrowski, B.; Freeland, J. W.; Shao-Horn, Y. Estimating Hybridization of Transition Metal and Oxygen States in Perovskites from O K-Edge X-Ray Absorption Spectroscopy. *J. Phys. Chem. C* **2014,** *118*, 1856-1863.

(20) Grimaud, A.; Carlton, C. E.; Risch, M.; Hong, W. T.; May, K. J.; Shao-Horn, Y. Oxygen Evolution Activity and Stability of $Ba_6Mn_5O_{16}$, $Sr_4Mn_2CoO_9$, and $Sr_6Co_5O_{15}$: The Influence of Transition Metal Coordination. *J. Phys. Chem. C* **2013,** *117*, 25926-25932.

(21) Qian, D.; Hinuma, Y.; Chen, H.; Du, L.-S.; Carroll, K. J.; Ceder, G.; Grey, C. P.; Meng, Y. S. Electronic Spin Transition in Nanosize Stoichiometric Lithium Cobalt Oxide. *J. Am. Chem. Soc.* **2012,** *134*, 6096-6099.

(22) Ferreira, P. J.; la O', G. J.; Shao-Horn, Y.; Morgan, D.; Makharia, R.; Kocha, S.; Gasteiger, H. A. Instability of Pt / C Electrocatalysts in Proton Exchange Membrane Fuel Cells: A Mechanistic Investigation. *J. Electrochem. Soc.* **2005,** *152*, A2256-A2271.

(23) Risch, M.; Ringleb, F.; Kohlhoff, M.; Bogdanoff, P.; Chernev, P.; Zaharieva, I.; Dau, H. Water Oxidation by Amorphous Cobalt-Based Oxides: In Situ Tracking of Redox Transitions and Mode of Catalysis. *Energy Environ. Sci.* **2015,** *8*, 661-674.

(24) Friebel, D.; Bajdich, M.; Yeo, B. S.; Louie, M. W.; Miller, D. J.; Sanchez Casalongue, H.; Mbuga, F.; Weng, T.-C.; Nordlund, D.; Sokaras, D.; Alonso-Mori, R.; Bell, A. T.; Nilsson, A. On the Chemical State of Co Oxide Electrocatalysts During Alkaline Water Splitting. *Phys. Chem. Chem. Phys.* **2013,** *15*, 17460-17467.

(25) Totir, D.; Mo, Y.; Kim, S.; Antonio, M. R.; Scherson, D. A. In Situ Co K‐Edge X‐Ray Absorption Fine Structure of Cobalt Hydroxide Film Electrodes in Alkaline Solutions. *J. Electrochem. Soc.* **2000,** *147*,

4594-4597.

(26) Tao, Y.; Zaijun, L.; Ruiyi, L.; Qi, N.; Hui, K.; Yulian, N.; Junkang, L. Nickel-Cobalt Double Hydroxides Microspheres with Hollow Interior and Hedgehog-Like Exterior Structures for Supercapacitors. *J. Mater. Chem.* **2012,** *22*, 23587-23592.

(27) Takamatsu, D.; Koyama, Y.; Orikasa, Y.; Mori, S.; Nakatsutsumi, T.; Hirano, T.; Tanida, H.; Arai, H.; Uchimoto, Y.; Ogumi, Z. First in Situ Observation of the $LiCoO_2$ Electrode/Electrolyte Interface by Total-Reflection X-Ray Absorption Spectroscopy. *Angew. Chem. Int. Ed.* **2012,** *51*, 11597-11601.

(28) Gardner, G. P.; Go, Y. B.; Robinson, D. M.; Smith, P. F.; Hadermann, J.; Abakumov, A.; Greenblatt, M.; Dismukes, G. C. Structural Requirements in Lithium Cobalt Oxides for the Catalytic Oxidation of Water. *Angew. Chem. Int. Ed.* **2012,** *51*, 1616-1619.

(29) Wang, Z. L.; Yin, J. S.; Jiang, Y. D. Eels Analysis of Cation Valence States and Oxygen Vacancies in Magnetic Oxides. *Micron* **2000,** *31*, 571-580.